Modeling the Synthesis of Amorphous $Si_3B_3N_7$ via a Sequence of Dynamically Well-Separated Steps

J. C. Schön,* A. Hannemann, and M. Jansen

Max-Planck-Institut für Festkörperforschung, Heisenbergstrasse 1, D-70569 Stuttgart, Germany

Received: September 2, 2003; In Final Form: December 2, 2003

The amorphous high-temperature ceramic a-$Si_3B_3N_7$ can only be synthesized via a sol−gel process. Here, we present a separation of time scales approach that can be used to model various aspects of the sol−gel process, resulting in a model for the synthesis as a sequence of dynamically well-separated steps. For chemically reasonable choices of process parameters in the actual implementation, we find satisfactory agreement with the structural data of the amorphous ceramic, in particular regarding the medium range order observed in NMR-experiments and the overall density.

1. Introduction

Among the most fascinating new materials for high-temperature applications have been the multinary nitrides and carbides such as a-$Si_3B_3N_7$ or a-$SiBN_3C$,[1−3] which exhibit an amazing high-temperature durability despite their amorphous structure. For example, a-$Si_3B_3N_7$ is stable up to $T_{dec} \approx 1900$ K when decomposition sets in, without any prior crystallization taking place. Even more remarkable is a-$SiBN_3C$ ($T_{dec} \approx 2100$ K), which is also highly stable in an oxygen atmosphere up to $T \approx 1700$ K. The elastic constants of these materials are relatively high (e.g., the bulk modulus of a-$SiBN_3C$ is $B = 200-300$ GPa), and despite their low density of about 1.8−1.9 g/cm^3, they exhibit a high breaking strength.

What are the physical and chemical reasons for these amazing properties? Because the materials are amorphous, the starting point for such an investigation must be the generation of appropriate microscopic structural models. In this work, we are going to focus on the prototypical ternary nitride a-$Si_3B_3N_7$, because its composition is well-defined, in contrast to, e.g., a-$SiBN_3C$, where a greater spread in composition is found. One major problem when trying to model these nitridic ceramics is the complicated synthesis route: First, precursor molecules such as TADB ($(SiCl_3)(NH)(BCl_2)$) are linked to oligomers via HCl elimination in NH_3, followed by a pyrolysis in N_2 atmosphere.[2,3]

Trying to exactly reproduce these processes in a straightforward simulation, analogous to a cooling from the melt used when modeling glasses, is nearly impossible. [And even when modeling glasses, the cooling rates are several orders of magnitude larger than the experimental ones.] Up to now, most of the theoretical work[4−13] in modeling the sol−gel process has focused on understanding the generic sol−gel transition, which was shown to be closely related to the lattice percolation problem.[10,14] The dynamic processes occurring during the gelation process have been extensively studied using the so-called kinetic gelation model,[11−16] where a small number of "monomers" are placed on a lattice, and then perform random walks generating the linked clusters of the evolving gel in the form of their traces on the lattice.

However, it is not clear, to what extent such simplified models are capable of mimicking the very complex synthesis routes encountered in the production of, e.g., an amorphous ceramic such as a-$Si_3B_3N_7$, in particular because the polymerization step is quite complex by itself and furthermore constitutes only one of the stages of the complete synthesis. Thus, it appears that the only way to model the synthesis of a-$Si_3B_3N_7$ is to break the complicated process into several pieces, where each step can be modeled or simulated in a simplified fashion. As a consequence, we have developed a multistage approach to address this problem.

In this work, we will first give a general outline of our approach, followed by details of our specific implementation. Next, the resulting structural models are analyzed with respect to the influence of various process parameters and finally compared with geometrical and topological information gained from physical measurements.

2. Sol-Gel Route

2.1. Experimental Observations. As mentioned above, a true simulation of the full sol−gel route is not yet feasible. To design the intermediate steps needed to construct a multistage model of the process, we first identify the central elements and stages of the actual synthesis route.

In the experiments, one starts with a dispersion of molecules containing (Si−N−B) units (TADB = $Cl_3Si-(NH)-BCl_2$) in a medium consisting of NH_3 molecules plus a certain amount of hexane. All components are highly mobile at this stage.

During polymerization, new bonds are being generated among and between these and the NH_3 molecules, removing the functional parts of the TADB molecules (the Cl atoms) and leaving only some hydrogen end groups:

$$\text{TADB} + NH_3 \rightarrow \text{polyborosilazane} + NH_4Cl \quad (1)$$

More specifically, the following reactions at the functional groups $(R_i)_mX-Cl$, $(R_i)_mX-NH_2$, and $(R_i)_mX-NH-Y(R_i)_n$ are likely to dominate the process:

$$(R_i)_mX - Cl + NH_3 \rightarrow (R_i)_mX - NH_2 + HCl \quad (2)$$

$$(R_i)_mX - Cl + (R_i)_nY - NH_2 \rightarrow (R_i)_mX - NH - Y(R_i)_n + HCl \quad (3)$$

$$(R_i)_mX - Cl + (R_i)_nY - NH - Z(R_i)_l \rightarrow ((R_i)_mX)((R_i)_nY)((R_i)_lZ)N + HCl \quad (4)$$

10.1021/jp036608m CCC: $27.50
Published on Web 01/23/2004

$$(R_i)_mX - NH_2 + (R_i)_nY - NH_2 \rightarrow (R_i)_mX - NH - Y(R_i)_n + NH_3 \quad (5)$$

$$(R_i)_m - NH - Y(R_i)_n + (R_i)_lZ - NH_2 \rightarrow ((R_i)_mX)((R_i)_nY)((R_i)_lZ)N + NH_3 \quad (6)$$

Here, X, Y, and Z can be B or Si and $(R_i)_m$, $(R_i)_n$, and $(R_i)_l$ just denote the remainder of the molecule containing the functional group. For X, Y, Z = B we have m, l, $n = 2$ and $i = 1$, 2, and for X, Y, Z = Si, we have m, l, $n = 3$ and $i = 1$, 2 and 3, respectively.

There exists only a limited amount of experimental and theoretical information regarding the details of these reactions. Presumably, reactions 5 and 6 are the slowest overall, whereas for identical $(R_i)_m$ and X, reaction 2 should be somewhat faster than reactions 3 and 4. Of particular interest has been the question, of how the speed of the aminolysis reactions 2−4 depend on the identity of X, and the details of the remainder R_1. Ab initio Car−Parrinello calculations have confirmed[17] the experimental knowledge that the (B−Cl) bond is more susceptible than the (Si−Cl) bond to aminolysis reactions because of the higher Lewis acidity of the former and that the details of $(R_i)_m$ are not crucial compared with the B vs Si effect.

Hexane does not appear to play any role in the actual reaction process; it only ensures that the final polyborosilazane remains soluble for the purpose of further processing (separation from the byproducts such as NH_4Cl, shaping, spinning, etc.) before the pyrolysis step. From the point of view of modeling the polymerization, the only effect of hexane is some reduction of the overall density of the reacting molecules.

Furthermore, we notice that this first reaction phase usually takes place in a considerable excess of NH_3, $c_{NH_3}/c_{TADB} = R_C \approx 100$. These conditions suggest that most of the Cl elimination will have taken place very early in the process before the actual cross-linking begins among the TADB molecules. Noting that each TADB contains five Cl atoms, one would estimate that the fraction of TADB molecules that are involved in n (≤ 5) reactions of type (3) and (4) is on the order of $O(R_C^{-n})$. [Most likely, this estimate is actually an upper limit, because the NH_3 molecules are much more mobile than oligomers containing more than one (Si−N−B)-unit. Thus, multiple encounters of TADB molecules needed to generate large oligomers early in the polymerization stage are even less likely once the local region around a TADB that has participated in several reactions has been depleted of TADB. Whether this effect makes a quantitative difference depends on the speed of reaction (2) compared to the speed of diffusion of the oligomers, of course. For a more precise analysis, the corresponding diffusion-reaction problem would need to be solved.]

Depending on R_C, one would expect that by the end of the Cl eliminiation only relatively small oligomers containing no more than on the order of ten (Si−N−B) units will be present. [A tree graph oligomer derived from m TADB molecules, i.e., containing m Si−N−B units occurs with probability $O(R_C^{-m})$. For $R_C = 100$ and $m = 10$, this leads to a probability $p = 10^{-20}$. Assuming 10^{21} TADB molecules immersed in 10^{23} NH_3 molecules leads to about ten $m = 10$ oligomers.] Further cross-linking should then occur via NH_3 elimination according to reactions 5 and 6.

Because the temperature is relatively low, many of the Si−N−B units from TADB are likely to survive intact at this polymerization stage. However, this is surely no longer going to be the case during the pyrolysis stage of the synthesis. During this pyrolysis in N_2, the remaining foreign atoms are removed while NH_3, N_2 and H_2 evolve, and the structure is allowed to solidify, becoming more dense in the process. This second process will also include the wholesale (local) destruction and rebuilding of the Si−N and B−N bonds, due to the high annealing temperatures (≈1500 K).

We conclude from our analysis that the central elements of the process are the following, where some overlap of these elements during the actual process is to be expected:

- Initial configuration
- Cl elimination
- Cross-linking with (X−Cl) functional groups still present (first stage)
- Cross-linking with only (X−NH_2) and (X−NH−Y) functional groups available (second stage)
- Pyrolysis

2.2. General Multistage Approach. *2.2.1. Initial Configuration.* We first note that the initial configuration can be modeled as being a random arrangement of the TADB, NH_3, and hexane molecules in a (periodically repeated) simulation cell. Furthermore, because hexane is inert for all practical purposes, it can be eliminated from the model. Thus, the initial configuration can be simplified and should only consist of TADB and NH_3, where all effects due to hexane are incorporated as a lowering of the initial density of the system. [In principle, the polymerization will also take place without any hexane being present.]

2.2.2. Cl Elimination. From the ab initio simulations, it appears that the details of the removal of the Cl atoms are probably not critical for the overall process. Here, we are only referring to possible differences in the reaction rates for the first, second, etc. Cl atom to be eliminated. The different reaction rates of B−Cl and Si−Cl bonds clearly need to be included in the model. For the simple model we are trying to construct, we will therefore ignore the Cl atoms by treating them as mere placeholders for free Si and B valencies. Similarly, the hydrogen atoms can be modeled as placeholders for free nitrogen valencies, in both TADB and ammonia.

Though it appears to be safe to discard the Cl and similarly the H atoms as such, a critical question is whether there exists a preference for the removal of Cl from the B or the Si functional unit. Similarly, we have to wonder whether free N valencies prefer to react with available Si or B valencies. Finally, there is the issue of whether free N valencies in TADB and oligomers (denoted N^1) react as quickly with free B or Si valencies as the free valencies in NH_3 (denoted N^2). From chemical experience, we expect that the reactivity of N^2 probably exceeds that of N^1 ($r(N^2) \geq r(N^1)$); within the approach presented here, we assume that the reactivity of N^1 and N^2 are comparable ($r(N^2) \approx r(N^1)$).

2.2.3. First Stage Cross-Linking. A first step to model this process would be to assume a very simplified interaction of molecules walking randomly inside the simulation cell: If a N with a free valency approaches a Si or B with a free valency, the two molecules link with a gain in energy $E_{Si-N} < E_{B-N}$, respectively. In the low-temperature regime of the polymerization process, we can even assume that any bond that has been formed is not going to be broken. Regarding the shape of the new molecule, we can assume that it obeys the simple model building rules for molecules, with N and B being approximately trigonally planar coordinated by cations and anions, respectively, and Si being tetrahedrally coordinated by N, with complete flexibility in the dihedral angles up to the point that two atoms collide within their van der Waals radii.

We note that B−N is the stronger bond, and thus one would assume that there will be a tendency to form B−N bonds over Si−N bonds. On the other hand, with B−N bonds having

perhaps formed quickly initially, they might be too stable to allow the formation of, e.g., a B−N−B linkage starting with two B−N bonds.

Ideally, we would perform long-term simulations, with a realistic ratio of the diffusion and reaction rates, and similarly realistic energy gains and costs for creating and destroying a B−N or Si−N bond. However, such a simulation is only feasible for a highly activated system, i.e., for unrealistic temperatures. A way to address this problem is a separation of time scales approach. At the beginning of the process, we can assume that the diffusion of all reaction participants is fast enough to create a homogeneous mixture (analogous to the well-stirred reactor approximation). No spatial variation of the reaction partners is present, and we can assume that the likelihood of each TADB to react with another TADB is exactly given by $1/R_C$. From the modeling point of view, this has another advantage: we can assume that, on the density-equilibration time scale, each TADB and NH_3 molecule moves randomly with arbitrary step length, i.e., each free spot in the simulation cell has equal probability to be the next location of the molecule.

However, we quickly encounter a problem regarding the movement of the newly linked molecules containing several Si−N−B units. Modeling the movement of these oligomers is rather expensive in computation time, in particular in a dense solution, where two such molecules are very slow to pass one another. A possible solution is to recall that the ammonia molecules are both highly mobile and present in excess. Thus we can assume that molecules consisting of more than N_{max} Si−N−B units are essentially stationary with respect to the medium, whereas the NH_3 molecules are always present everywhere in the system as before. Once cross-linking has started and produced larger molecules, these serve as spatially fixed growth centers for the further adsorption of TADB and ammonia molecules.

One issue we have to address at this stage is the faster reactivity of B−Cl functional groups. If we assume that the individual TADB molecules can quickly rotate in the NH_3 medium, the opportunity to react can be taken as equal for all functional groups, B−Cl and Si−Cl, and the likelihood that a successful reaction takes place depends on the reaction rates. Thus, free B valencies will more quickly be saturated than the Si valencies, both at the stationary oligomers and the still mobile TADB.

2.2.4. Second Stage Cross-Linking. After all free B and Si valencies have been saturated, two things change. The NH_3 molecules can no longer react, and the reaction rates will presumably be slower than before, because only reactions 5 and 6 can take place. Thus, we can from now on ignore the NH_3 molecules, while continuing to move single TADB molecules and perhaps also small oligomers. Now reactions 5 and 6 will occur among the stationary oligomers and mobile TADB, where we still assume that at the low temperatures where the polymerization is performed no B−N or Si−N bond will break, at least not without being re-formed right away during the ammonolysis.

Once all TADB molecules have become part of stationary oligomers, the separation of time scales arguments cut the other way. Now the diffusion (and "wobbling") of the oligomers will be the slow controlling time scale, whereas we assume that the (irreversible) reaction takes place at once after the encounter of two oligomers. In principle, we can now perform an appropriate diffusion simulation for the oligomers. However, there is a faster way: Reducing the density by rescaling the simulation cell leads for the small clusters to get within range of another, and results in the desired merger dynamics of the small oligomers.

We note that, implicitly, this model assumes that growth takes place essentially continuously without any breaking of bonds. This favors a "first seen, first bonded" approach, only modified by the special model kinetics favoring the saturation of the free B valencies. However, for very long polymerization times in the real system, one might want to permit bond-breaking, too. In this way, the relative strengths of the B−N and Si−N bonds mentioned earlier can also be taken into account.

Still, these statistically relevant properties of the system would not make themselves felt during the relatively short MC/MD simulations we can perform. Annealing at low temperatures is too slow for the statistical preference to preserve B−N bonds, to have an effect compared to the influence of the initial random placement; after all, Si−N bonds are also very strong by themselves and do not break easily at low temperatures once they have formed. [Of course, in the melt at high temperatures, we clearly notice the higher strength of the B−N bond, even on short time scales.[18] But such high temperatures are not part of the sol−gel route we would like to model.] Of course, we can take this tendency, i.e., for stronger B−N bonds to be present with a higher probability, into account by again favoring reactions 5 and 6 for X = B over X = Si during the merger dynamics.

2.2.5. Pyrolysis. Although at the beginning of the pyrolysis phase we can still use the modeling procedure from the previous step, this no longer holds true for the long-time annealing at higher temperatures. Although the available simulation times are still rather short, we can now perform MC or MD simulations at the annealing temperature $T \leq 1500$ K, using satisfactory empirical potentials.

2.3. Implementation. *2.3.1. General Aspects.* In our implementation, we have decided to model polymerization and the early stage of the pyrolysis in one step, to focus on the kinetic effects. We assume that, on the long time scales we are interested in, many openings and closings of Si−N and B−N bonds can take place. Thus, concepts from statistical mechanics can be applied: We can assume that the Si−N−B unit can be destroyed and, furthermore, the addition of new atoms and the growth of the polymer clusters can be modeled by assuming an enhanced average sticking probability of B atoms at free N atom valencies.

In addition, we note that the larger the oligomers and polymers have become, the less likely they are to move past each other in the solution. On the other hand, the individual molecules and atoms that attach to the larger units are still quite mobile and thus can be assumed to be homogeneously dispersed throughout the volume. The assumption of many bond breakings and openings allows us to model the growth of these polymers as an aggregation-growth process, where no atom that has been linked to the polymer is ever removed again. [Of course, in reality, an individual atom could be added and removed many times. But statistically, there will always be some atom present at the bonding site once an atom has been added a first time. Thus, the (pieces of the) polymer only grow and never diminish when viewed on the long time scale on which short time fluctuations have been averaged out.]

Because this process will take place throughout the volume, we assume that several starting centers are present, where the growth process will be initiated. The kinetic effect makes itself felt in the preference of nonsaturated N atoms at the surface of the polymer to preferentially bond to the available B atoms. One should also note that we are in a highly oversaturated state

and that the density of the oligomers is so high that the final fully linked compound is created by a merger dynamics[19] of these small polymer pieces, and not via an Ostwald-ripening process.

2.3.2. Algorithmic Implementation. To implement this procedure, we proceeded as follows: We started with a periodic (to take the essentially infinite extent of the real system into account) diamond-type lattice, where the number of sites in the simulation cell was such that a prescribed density was going to be achieved upon the placement of all $N_{atom} = N_{Si} + N_B + N_N$ atoms. The distance between two neighboring lattice sites corresponded to the average of the B−N and Si−N bond lengths (1.54 Å). A small percentage of the (Si, N, and B) atoms were placed onto the lattice to serve as aggregation initiation sites. Next, we swept over all anions and cations already on the lattice and added one cation or anion from the reservoir, respectively, to an open neighboring lattice point of the atom under consideration. Of course, we ensured that the topology was correct, i.e., only up to three neighbors for B and N and up to four for Si were allowed, respectively, and similarly no cation−cation or anion−anion nearest neighbors were permitted. This applied to both the site at which the atom was inserted and the occupied neighbor sites. The kinetic effect was taken into account by giving a preference to B atoms whenever it was a N atom's "turn" to choose a new neighbor, while ensuring that the final composition was as desired ($N_{Si} = N_B$). After each insertion of a B or Si atom, we update the bonding probabilities p_{N-B} ($=1 - p_{Si-N}$),

$$p_{N-B}(n+1) = \frac{N_B^r}{N_B^r + N_{Si}^r} p_{N-B}(n) \qquad (7)$$

where N_{Si}^r and N_B^r are the number of silicon and boron atoms in the reservoir, respectively. The initial value of p_{N-B} was denoted p_{N-B}^0.

As long as the prescribed final density was not too high, this process only stopped after all N_{atom} atoms have been placed. Thus, we chose a density of $\rho^{init} = 1.57$ g/cm^3, which is consistent with the density at the beginning of the pyrolysis stage of the actual synthesis ($\rho = 1-1.4$ g/cm^3 [20]). Using this procedure, we generated five structures each for two sizes of the initial atoms set (3 and 30). [For consistency checks, we also generated structures with 15 growth centers for selected values of p_{N-B}.]

The final two steps modeled the annealing phase of the pyrolysis. First, we removed the strains introduced by the lattice-based growth procedure, by a constant volume local optimization followed by a constant pressure conjugate gradient local optimization. [We chose to keep the volume constant during this step, because at this stage there should still be a sufficient internal pressure to keep the network from collapsing, due to the evolving gas (H_2, Cl_2, N_2, and NH_3). Once all gas molecules had been removed from the system, this counterbalancing force was removed, and the density was left to be optimized using a constant pressure conjugate gradient relaxation.] The optimizations employed the computationally efficient two-body interaction potential *A*[21] where the interaction went smoothly to zero at the atom−atom distance of 6 Å $E_{pot}^A = \sum_{i \neq j}^{N_{atom}} V_{ij}^A$. [Because the specific form of the potential is rather complex, we refer to the literature[21] for further details.]

2.3.3. Pyrolysis. We modeled the final stage of the pyrolysis by Monte Carlo relaxations at different temperatures between 250 and 3000 K, in which we varied both the cell parameters and the atomic positions at zero external pressure. For the MC relaxations we employed again the interaction potential *A*. The run length of the simulations was 10^6 Monte Carlo cycles (MCC), and we varied the cell parameters isotropically every 100 MCC on average. [The effect of the frequency of the cell parameter moves was investigated, but no noticeable effects on the final structures were found.] Here, one MCC consisted of *N* atomic displacements. The final tempered configurations were again optimized by conjugate gradient local optimizations in which both the cell parameters and the atomic positions were simultaneously optimized and we refined the optimized models using a reverse Monte Carlo (RMC)[22] stochastic quench procedure. In the latter, the cost function $C(\vec{r}_i;\lambda)$ was given as a linear combination of the difference between the computed [see refs 23 and 24 for details on the computation of the pair correlation functions for atomistic models] and experimentally measured (via X-ray or neutron scattering) radial distribution function $(\Delta R_B(\vec{r}_i))^2$ and the potential energy $E_{pot}^A(\vec{r}_i)$,

$$C(\vec{r}_i;\lambda) = \lambda(\Delta R_B(\vec{r}_i))^2 + (1-\lambda)E_{pot}^A(\vec{r}_i) \qquad (8)$$

We chose $\lambda = 0.2$ on the basis of our experience from earlier work.[25] [The RMC-quench procedure is only used as a refinement step. For $\lambda = 0.2$, one obtains a maximum refinement without losing the results from the energy minimization.] Typically, the changes in the atom positions in this final refinement step were minute (<0.001 Å/atom), and the overall topology of the network did not change.

TABLE 1: Mean Coordination Numbers of Silicon (Si), Boron (B) and Nitrogen (N) of the Models at the End of the Growth Stage Prior to Pyrolysis and Mean Number of Si−Si, Si−B, B−B, and B−Si Next-Nearest Neighbors of the Models at the End of the Growth Stage Prior to Pyrolysis[a]

(a) nearest neighbors					(b) next nearest neighbors					
p_{N-B}^0	I	Si	B	N	p_{N-B}^0	I	Si−Si	Si−B	B−B	B−Si
0.50	3	3.77	2.11	2.52	0.50	3	4.69	1.79	1.81	1.79
0.50	30	3.42	1.95	2.30	0.50	30	3.49	1.92	1.19	1.92
0.70	3	3.39	2.35	2.46	0.70	3	3.45	2.19	1.76	2.19
0.70	30	3.11	2.19	2.27	0.70	30	2.88	1.92	1.52	1.92
0.80	3	3.10	2.55	2.42	0.80	3	2.75	2.37	1.87	2.37
0.80	30	2.90	2.37	2.26	0.80	30	2.41	2.06	1.69	2.06
0.90	3	2.79	2.76	2.38	0.90	3	2.33	2.09	2.51	2.09
0.90	30	2.59	2.62	2.23	0.90	30	2.00	1.93	2.18	1.93
0.95	3	2.67	2.86	2.37	0.95	3	2.48	1.66	3.20	1.66
0.95	30	2.38	2.79	2.22	0.95	30	1.77	1.73	2.71	1.73
0.99	3	2.59	2.92	2.36	0.99	3	2.65	1.19	3.99	1.19
0.99	30	2.28	2.86	2.20	0.99	30	1.58	1.58	3.16	1.58

[a] p_{N-B}^0 is the initial probability to bind a nitrogen atom to a boron atom. *I* is the number of atoms initially placed on the lattice.

3. Results

3.1. Polymerization and Pyrolysis. Table 1 shows the distribution of nearest and next-to-nearest neighbors in the oligomers generated at the end of the growth stage. Table 2 presents the same quantities after the subsequent constant volume plus subsequent constant pressure conjugate gradient minimizations, corresponding to the initial stage of the pyrolysis. Finally, Table 3 shows the mean coordination numbers after the RMC-quench refinement. In the first coordination spheres, boron and silicon were coordinated by 2.6−3.0 and 3.6−4.0 nitrogen atoms, respectively, and nitrogen was coordinated by about 2.8−2.9 cations. We only observe a relatively small dependence on the probability to form N−B bonds, p_{N-B}^0, and on the number of growth centers *I*: Larger values of p_{N-B}^0 resulted in higher/lower coordination of B/Si by nitrogen, and variations in the number of starting sites did not lead to

TABLE 2: Mean Coordination Numbers of Silicon (Si), Boron (B), and Nitrogen (N) of the Models after the First Stage of the Pyrolysis and Mean Number of Si−Si, Si−B, B−B, and B−Si Next-Nearest Neighbors of the Models after the First Stage of the Pyrolysis, i.e., after the Conjugate Gradient Minimizations[a]

(a) nearest neighbors						(b) next nearest neighbors					
p^0_{N-B}	I	Si	B	N	ρ_{opt}	p^0_{N-B}	I	Si−Si	Si−B	B−B	B−Si
0.50	30	3.97	2.58	2.81	1.65	0.50	30	5.12	2.78	2.07	2.78
0.50	3	4.04	2.53	2.82	1.57	0.50	3	5.56	2.26	2.55	2.26
0.70	30	3.91	2.70	2.83	1.68	0.70	30	4.83	3.00	2.16	3.00
0.70	3	3.95	2.71	2.85	1.61	0.70	3	4.92	2.96	2.30	2.96
0.80	30	3.86	2.80	2.85	1.72	0.80	30	4.57	3.25	2.24	3.25
0.80	3	3.87	2.82	2.87	1.70	0.80	3	4.48	3.30	2.20	3.29
0.90	30	3.77	2.87	2.85	1.72	0.90	30	4.47	3.16	2.48	3.16
0.90	3	3.77	2.91	2.86	1.62	0.90	3	4.59	3.05	2.66	3.05
0.95	30	3.74	2.95	2.87	1.74	0.95	30	4.61	3.03	2.87	3.03
0.95	3	3.73	2.97	2.87	1.62	0.95	3	5.07	2.59	3.29	2.59
0.99	30	3.70	2.97	2.86	1.79	0.99	30	4.61	2.83	3.29	2.83
0.99	3	3.74	2.98	2.88	1.67	0.99	3	5.62	2.11	3.99	2.11
exp		3.4−3.8	2.8−3.0	2.6−3.0	1.9	exp		6	1.7−1.9	4(−5)	1.3−1.5

[a] p^0_{N-B} is the initial probability to bind a nitrogen atom to a boron atom. *I* is the number of atoms initially placed on the lattice. ρ_{opt} is the density of the models after polymerization.

TABLE 3: Mean Coordination Numbers of Silicon (Si), Boron (B), and Nitrogen (N) of the Models after the RMC-Quench Refinement and Mean Number of Si−Si, Si−B, B−B, and B−Si Next-Nearest Neighbors of the Models after the RMC-Quench Refinement[a]

(a) nearest neighbors					(b) next nearest neighbors					
p^0_{N-B}	I	Si	B	N	p^0_{N-B}	I	Si−Si	Si−B	B−B	B−Si
0.50	3	3.90	2.54	2.76	0.50	30	4.55	2.63	2.07	2.63
0.50	30	3.79	2.58	2.83	0.50	3	5.13	2.16	2.56	2.16
0.70	3	3.74	2.71	2.77	0.70	30	4.28	2.82	2.16	2.82
0.70	30	3.73	2.70	2.75	0.70	3	4.31	2.77	2.30	2.77
0.80	3	3.65	2.82	2.77	0.80	30	3.91	3.03	2.23	3.03
0.80	30	3.63	2.80	2.76	0.80	3	3.89	3.06	2.20	3.06
0.90	3	3.56	2.91	2.77	0.90	30	3.81	2.94	2.47	2.94
0.90	30	3.56	2.87	2.76	0.90	3	3.93	2.85	2.66	2.85
0.95	3	3.51	2.96	2.78	0.95	30	3.89	2.80	2.85	2.78
0.95	30	3.49	2.94	2.76	0.95	3	4.29	2.43	3.28	2.42
0.99	3	3.50	2.97	2.78	0.99	30	3.88	2.58	3.25	2.56
0.99	30	3.46	2.95	2.76	0.99	3	4.76	1.93	3.96	1.92

[a] p^0_{N-B} is the initial probability to bind a nitrogen atom to a boron atom. *I* is the number of atoms initially placed on the lattice.

significant changes. Note that the densities of the optimized models is in all cases around 1.7 g/cm^3, close to the experimentally observed density of 1.9 g/cm^3.

The effect of p^0_{N-B} is more visible in the second coordination sphere, where, e.g., larger values of p^0_{N-B} result in higher B−B next nearest neighbor coordinations. Again, no clear dependence on the number of the initially placed atoms *I* is found.

Quite generally, the relative values of the mean coordination numbers are similar at the end of the growth stage and at the end of the first part of the pyrolysis. The difference lies in the larger number of "dangling" bonds before the onset of pyrolysis, due to the not-yet-saturated valencies of the oligomers.

Parts a and c of Figure 1 show the computed X-ray and neutron diffraction radial distribution functions in comparison with experiment, before a RMC refinement. In both cases, already good qualitative agreement with experiment is observed, which improves even more once the RMC refinement is performed (cf. Figure 1b,d). As function of p^0_{N-B}, the agreement appears to be higher for higher values of p^0_{N-B}, for both X-ray and neutron data. As mentioned earlier, the topology of the structure does not change significantly in the RMC refinement step.

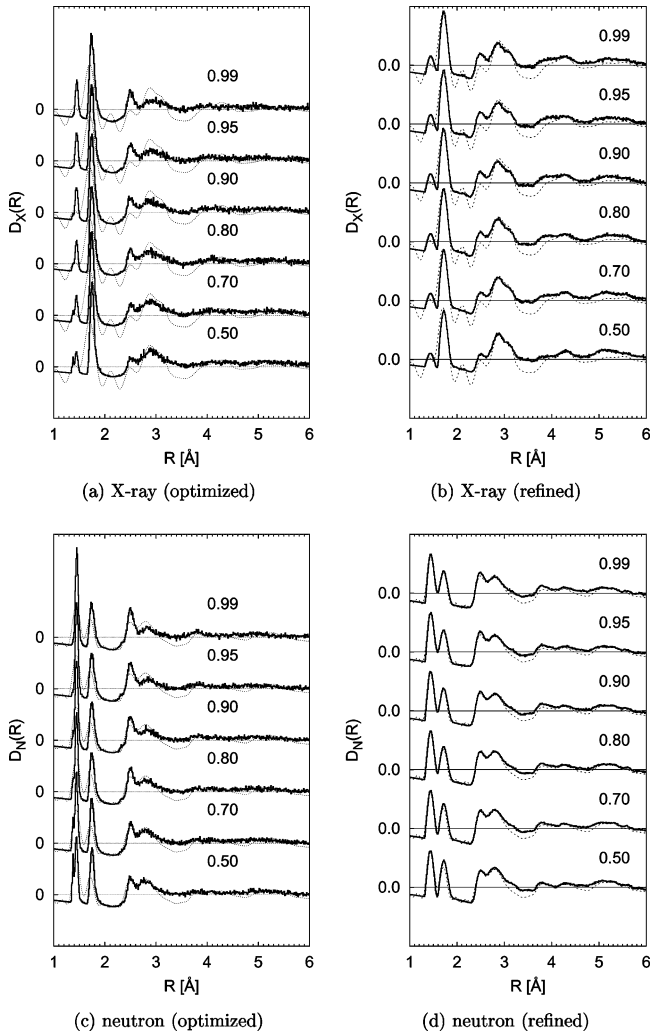

Figure 1. X-ray (top) and neutron (bottom) pair correlation functions of the constant pressure optimized structural models (left column) and the RMC-refined models. Dotted line shows the experimental data. Numbers inside the figures are the values p^0_{N-B}. The number of initially placed atoms was 30.

Next, we present the angle distributions at Si, B, and N (cf. Figure 2). We observe only relatively small effects of the choice of p^0_{N-B}, mostly in the strength of the 90° peak in the N−Si−N angle distribution, which indicates the presence of edge-sharing

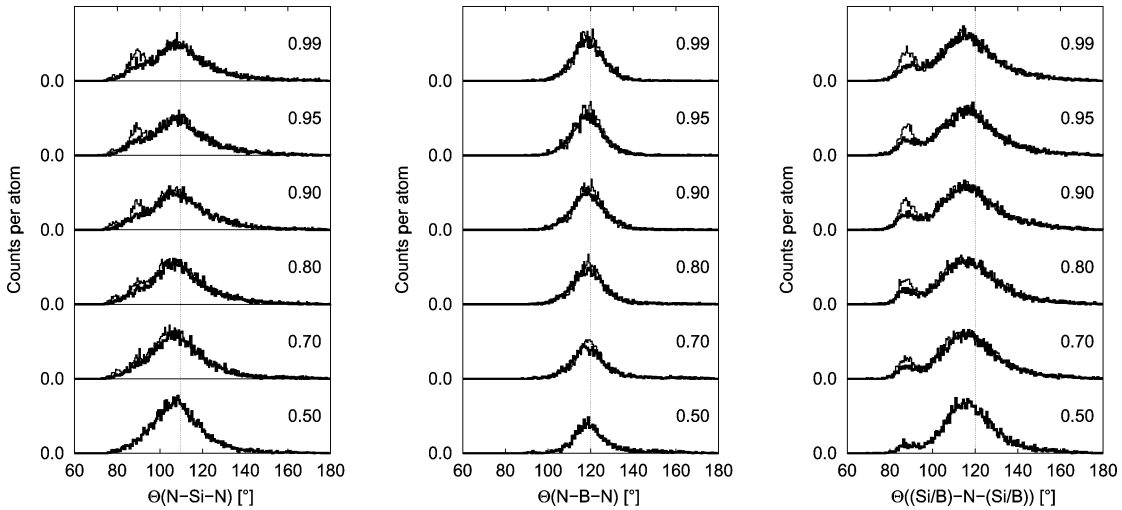

Figure 2. Angular distribution function of silicon (left), boron (middle), and nitrogen atoms (right) before (thin lines) and after (bold lines) RMC refinements of the constant pressure optimized models. The number of initially placed atoms was 30.

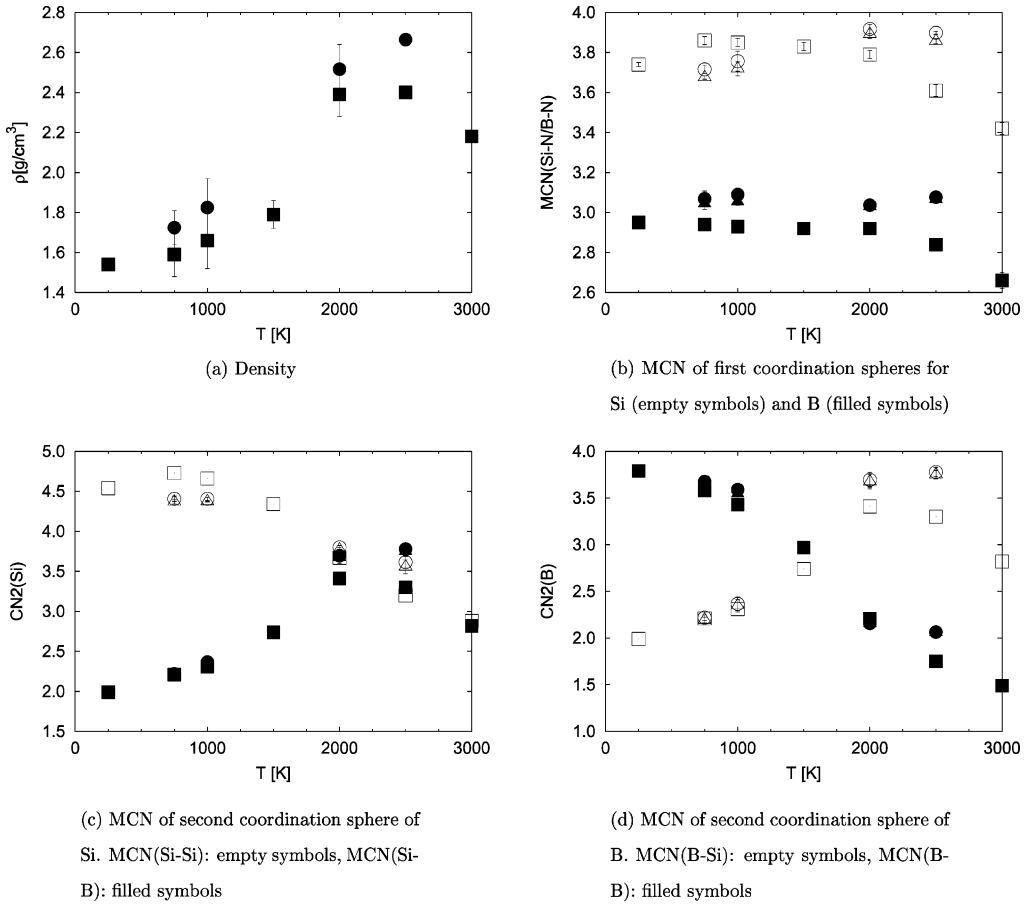

Figure 3. Temperature dependence of various properties of the annealed models (density, mean coordination numbers (MCN) of Si and B in the first and second coordination spheres). Squares represent the data of an average taken over configurations along the trajectory during tempering, circles are the data of the energy-optimized models, and triangles are the data for the RMC-refined models.

among the SiN_4 tetrahedra. Note that this effect is less pronounced for the RMC-refined models.

3.2. Annealing Stage of the Pyrolysis. Finally, we turn to the structures of the models one finds after tempering for 10^6 MCC at various temperatures at zero external pressure. We have tempered only those models that were generated using an initial bonding probability $p^0_{N-B} = 0.99$ at different temperatures $T \leq 4000$ K.

Parts a−d of Figure 3, depicting the temperature dependences of different structural and bulk properties of the tempered (squares), the constant pressure optimized (circles), and the refined models (triangles), show that these properties change significicantly once the temperature was raised above 1500 K. Below 1500 K the density of the structure increased only slightly, reaching a value of 1.8 g/cm^3, close to the experimentally found value. Similarly, we find that the mean coordination numbers for the first coordination sphere are essentially preserved up to 1500 K, only an increase is observed, whereas the second coordination number only changes weakly up to 1500 K (Figure 3b,c).

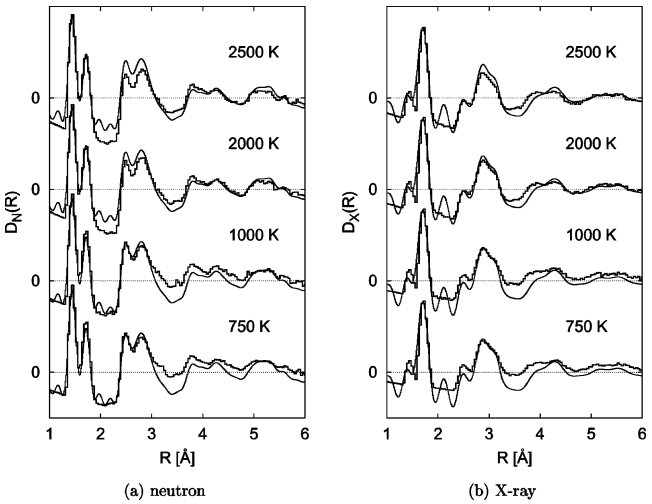

Figure 4. Neutron (left) and X-ray (right) pair correlation functions of the tempered structural models after constant pressure local optimizations and RMC refinement. The temperatures at which the models were tempered are given inside the figures. Thin lines represent the experimental data, where the small peaks up to 2.3 Å are artifacts of the measurement and analysis process (ghost peaks).

Above 1500 K, the higher number of boron−boron next nearest neighbors as well as silicon−silicon next nearest neighbors vanishes. We note here that neither the optimization nor the RMC refinements change the structural and bulk properties significantly, which are in agreement with the experimental data. This holds also for the pair correlation functions, which continue to show good agreement with experimental data (Figure 4). Note that the agreement between the experimental and the pair correlation functions of the "high temperature" models is slightly better than for the "low temperature" models. In contrast, the densities and the numbers of next nearest neighbors of the "low temperature" models agree better with the experimental data.

4. Discussion

In the previous sections we have presented a multistage implementation of a separation of time scales approach to the modeling of a-$Si_3B_3N_7$. The agreement of theory and experiment for the pair correlation functions derived for neutron and X-ray scattering is satisfactory. Silicon- and boron-rich regions are present in the final ceramic after annealing and have also been observed in NMR experiments.[26,27] Furthermore, the densities of the generated models are very close to the experimental density.

We note that the cavities generated in the polymerization and merger stage (which are the reason for the low final density) prove to be quite stable even during the annealing at up to 1500 K. The reason is most likely that the procedure yields rather compact oligomers before the merger stage and the subsequent annealing. Here, one should keep in mind the fact that in the experiment the overall volume can only decrease via the diffusion of voids to the surface of the material. But once a crust has formed, i.e., all voids within the first few nanometers have been removed, this process stops and the density remains essentially unchanged for the remainder of the annealing. In contrast, during the simulations void space can be removed rather easily[28] (the surface is "effectively" only about 20 Å away!). Thus, the increase of the density during the annealing tends to greatly exaggerate the effect. [In other work,[28] we have shown in simulations for larger system sizes (5200 atoms) that voids of radius $R_p = 8$ Å remain stable up to 1500 K.] Here, we also note that the structural properties of the annealed models are rather insensitive to the annealing at temperatures $T < 1500$ K, again showing that the synthesis route and the kinetics involved do play an important role for the structural properties of the synthesized product.

Considering the formation of silicon- and boron-rich regions, the kinetic effect incorporated by the preferred bonding probabilities p_{N-B} is clearly visible, in that both silicon- and boron-rich islands are formed. However, for larger distances from the individual growth centers, a more homogeneous cation distribution on length scales exceeding 10 Å should develop to be in agreement with experiment.[29] Clearly, a strongly biased purely atomistic growth process could easily lead to very large heterogeneities. A likely solution is that only relatively small clusters form initially, which then merge during the gelation stage. Within the context of our modeling approach, this would correspond to the existence of a rather large number of aggregation sites per volume. This choice of parameters is also consistent with our general considerations that motivated the separation of time scales approach, where the reactions among the TADB molecules and the NH_3 molecules are expected to occur at a multitude of locations throughout the solution; i.e., we do not deal with a standard nucleation and growth process as one would expect to occur during a synthesis via the cooling from the melt.

Of course, one would prefer to employ parameter values for reactivities and diffusion constants that are directly based on experimental measurements of reaction and diffusion rates of the participating molecules in the liquid ammonia plus hexane solution. Furthermore, such quantitative information would allow us to refine our general approach and help us to better identify and model the central stages of the synthesis. Up to now, however, such data are lacking, and one can, at best, reason by analogy. E.g., a comparison of diffusion constants $D_1 \approx 1.2 \times 10^{-5}$ cm^2/s and $D_2 \approx 2 \times 10^{-5}$ cm^2/s of methanol[30] and H_2O[31] in water with the diffusion constants $D_N \approx 10^{-6}-10^{-12}$ cm^2/s of polymer molecules in methanol[32] shows that D_1 and D_2 are the same within a factor of 2, whereas the latter D_N are several of orders of magnitude larger (depending on the size of the polymer molecules, of course). Picturing methanol and H_2O in the roles of TADB and NH_3, this supports our assumption that after a certain amount of growth has taken place, the oligomer can be treated as essentially stationary compared with the NH_3 and TADB molecules. Clearly, measurements of reaction rates of, e.g., $SiCl_4$ and BCl_3 in ammonia and of TADB molecules with NH_3 and each other, and of diffusion rates of TADB-derived oligomers in both NH_3 and mixtures of NH_3 with larger molecules, would be highly desirable.

A second class of experiments that would allow us to validate and improve the details of our stepping stone approach consist of in situ measurements of various quantities while the synthesis progresses, possibly with a very high time resolution. Such quantities might be the number of reaction centers per volume and the average size of the individual oligomers reflected in the atomic weight distributions of the developing polymer, the number of NH_2/NH/H/Cl-reactive moieties per oligomer, or the cation distribution in (individual) oligomers, which might be accessible by NMR experiments. Such measurements could be compared with the data given in, e.g., Tables 1−3.

A comparison of the final structures with those one finds when simulating alternative synthesis routes, such as glass formation from the melt, sintering of nanosized crystal fragments,[33] or random close packing analogous to vapor deposi-

tion,[25] shows that the structures presented here compare favorably with those other models, both regarding the pair correlation functions and with respect to medium range order and the density (for more details, see ref 34). Only the crystal fragment model exhibits similarly good agreement with experimental data.

Finally, the separation of time scale approach we have presented here is very general, of course, and can be easily modified to model the sol−gel synthesis of other amorphous solids. In such modifications, one could also include solvent effects, details of the participating monomers, or concurrent growths of larger building units, and thus obtain an in-depth view into the genesis of inorganic polymers.

Acknowledgment. We thank T. Jäschke for many valuable discussions of the chemical processes during the synthesis of silicon boron nitride. Funding was kindly provided by the DFG via SFB408.

References and Notes

(1) Baldus, P.; Wagner, O.; Jansen, M. *Mater. Res. Soc. Symp. Proc.* **1992**, *271*, 821−826.
(2) Baldus, P.; Jansen, M.; Sporn, D. *Science* **1999**, *285*, 699−703.
(3) Jansen, M.; Sporn, P. *Angew. Chem., Int. Ed. Engl.* **1997**, *36*, 328−343.
(4) Flory, P. J. *J. Am. Chem. Soc.* **1941**, *63* (11), 3083−3090.
(5) Flory, P. J. *J. Am. Chem. Soc.* **1941**, *63* (11), 3090−3096.
(6) Flory, P. J. *J. Am. Chem. Soc.* **1941**, *63* (11), 3096−3100.
(7) Stockmayer, W. H. *J. Chem. Phys.* **1943**, *11* (2), 45−55.
(8) Stockmayer, W. H. *J. Chem. Phys.* **1944**, *12* (1), 125−131.
(9) Zimm, B. H.; Stockmayer, W. H. *J. Chem. Phys.* **1949**, *17* (10), 1301−1314.
(10) de Gennes, P. G. *J. Phys. Lett.* **1976**, *37*, L1-L2.
(11) Herrmann, H. J.; Stauffer, D.; Landau, D. P. *J. Phys. A: Math. Gen.* **1983**, *16*, 1221−1239, 1983.
(12) Herrmann, H. J. *Phys. Rep.* **1986**, *136* (3), 153−227.
(13) Liu, Y.; Pandey, R. B. *Phys. Rev. B* **1997**, *55* (13), 8257−8266.
(14) Stauffer, D. *J. Chem. Soc., Faraday Trans. 2* **1976**, *72*, 1354−1364.
(15) Liu, Y.; Pandey, R. B. *J. Phys. II* **1994**, *4*, 865−872.
(16) Pandey, R. B.; Liu, Y. *J. Sol-Gel Sci. Technol.* **1999**, *15*, 147−159.
(17) Reinhardt, S.; Marian, C. M.; Frank, I. *Angew. Chem., Int. Ed. Eng.* **2001**, *40* (19), 3683.
(18) Schön, J. C.; Hannemann, A.; Sethi, G.; Jansen, M.; Salamon, P.; Frost, R.; Kjeldgaard, L. Proc. XXIII Workshop on structure and kinetics of nucleation and crystallization in noncrystalline materials, Jena September 2002; also as: cond-mat/0212279, 2002.
(19) Kjeldgaard, L.; Schön, J. C *J. Phys.: Condens. Matter* **1994**, *6* (36), 7269−7286.
(20) Jäschke, T. Ph.D. Thesis, Universität Bonn, Shaker Verlag Aachen, 2002.
(21) Gastreich, M.; Marian, C. M.; Gale, J. D. *Phys. Rev. B* **2000**, *62*, 3117−3123.
(22) Keen, D. A.; McGreevy, R. L. *Nature* **1990**, *344*, 423−425.
(23) Elliott, S. R. *Physics of Amorphous Materials*; Longman Scientific & Technical: Essex, U.K., 1990.
(24) Lamparter, P.; Steeb, S. *Materials Science and Technology: Structure of Solids*; VCH: Weinheim, 1993; Chapter 4, pp 217−288.
(25) Hannemann, A.; Schön, J. C.; Jansen, M. *Comput. Phys. Commun.* **2002**, *144*, 284−296.
(26) van Wüllen, L.; Müller, U.; Jansen, M. *Chem. Mater.* **2000**, *12* (8), 2347−2352.
(27) van Wüllen, L.; Müller, U.; Jansen, M. *Angew. Chem., Int. Ed. Eng.* **2000**, *39* (14), 2519−2521.
(28) Hannemann, A.; Schön, J. C.; Jansen, M. Manuscript in preparation.
(29) Heinemann, D.; Assenmacher, W.; Mader, W.; Kroschel, M.; Jansen, M. *J. Mater. Res.* **1999**, *14* (9), 3746−3753.
(30) Weast, R., et al., Eds. *CRC Handbook of Chemistry and Physics*, 70th ed.; The Chemical Rubber Company: Cleveland, OH, 1989.
(31) Pietsch, E. H. E., et al., Eds. *Gmelin Handbuch der Anorganischen Chemie "Sauerstoff"*; Gmelin Institute: Frankfurt, 1963; no. 3, Liefer. 5.
(32) Rietveld, I. B.; Bedeaux, D. *Macromol.* **2000**, *33*, 7912−7917.
(33) Hannemann, A.; Schön, J. C.; Oligschleger, C.; Jansen, M. In *Proceedings of DGK-workshop on 'Struktur und Eigenschaften nichtkristalliner Materialien − Messdaten und Strukturmodelle' (Wolfersdorf Sept. 1999)*; Müller, B., Ed.; University of Jena: Jena, 1999; also cond-mat/0001319.
(34) Hannemann, A.; Schön, J. C.; Putz, H.; Lengauer, T.; Jansen, M. Submitted to *Phys. Rev. B*, 2003.